# Dalton Transactions

Accepted Manuscript






ROYAL SOCIETY OF CHEMISTRY

www.rsc.org/dalton

Dalton Transaction

RSCPublishing

ARTICLE

# In-situ characterization of uranium and americium oxide solid solution formation for CRMP process: first combination of in-situ XRD and XANES measurements

Cite this: DOI: 10.1039/x0xx00000x

Received 00th January 2012,
Accepted 00th January 2012

DOI: 10.1039/x0xx00000x

www.rsc.org/

Marie Caisso[1,2,7], Sébastien Picart[2], Renaud C. Belin[3], Florent Lebreton[1], Philippe M. Martin[4], Kathy Dardenne[5], Jörg Rothe[5], Daniel R. Neuville[6], Thibaud Delahaye[2,*], André Ayral[7]

Transmutation of americium in heterogeneous mode through the use of $U_{1-x}Am_xO_{2\pm\delta}$ ceramic pellets, also known as Americium Bearing Blankets (AmBB), has become a major research axis. Nevertheless, in order to consider future large-scale deployment, processes involved in the AmBB fabrication have to minimize fine particles dissemination, due to americium presence, which considerably increases the risk of contamination. New synthesis routes avoiding the use of pulverulent precursors are thus currently under development, such as the Calcined Resin Microsphere Pelletization (CRMP) process. It is based on the use of weak-acid resin (WAR) microspheres as precursors, loaded with actinide cations. After two specific calcinations under control atmospheres, resin microspheres are converted into oxide microspheres composed of a monophasic $U_{1-x}Am_xO_{2\pm\delta}$ phase. Understanding the different mechanisms implied during thermal conversion, leading to the release of organic matter and the formation of a solid solution, appeared essential. By combining in-situ technics such as XRD and XAS, it has become possible to identify the key temperatures for oxide formation, and the corresponding oxidation states taken by uranium and americium during mineralization. This paper thus presents the first results on the mineralization of (U,Am) loaded resin microspheres into a solid solution, through in-situ XAS analysis correlated with HT-XRD.

## Introduction

Improve safety standards, sustainably optimize radioactive material management and minimize waste production are the foundations of the fourth-generation-reactor project ASTRID (Advanced Sodium Technological Reactor for Industrial Demonstration). This French prototype of sodium-cooled Fast Neutron Reactor (FNR) is being designed to assess the capacity of fast neutron reactors to burn plutonium isotopes.[1] In an ongoing commitment to close nuclear fuel cycle, it will also be used for experimental studies focused on minor actinide (MA) transmutation.[2] Indeed, at the back-end of the cycle, MA receive major consideration from the French authorities, as they remain, after plutonium reprocessing in MOX ($(U,Pu)O_2$ mixed oxide) fuel,[3] the most hazardous long-term components of nuclear waste far ahead short-lived fission products. Research on partitioning and transmutation has begun in France since the adoption of the Bataille act, in 1991, and is one of the studied options to optimize the final waste management by producing shorter half-lived or inactive chemical elements after their irradiation in FNR. Over the past few years, transmutation of only americium in heterogeneous mode through the use of $U_{1-x}Am_xO_{2\pm\delta}$ compounds has progressively been considered as a reference with the elaboration of Americium Bearing Blankets (AmBB),[4] under the form of dense ceramic pellets with a U/Am ratio of 90/10. New routes have currently shown

the feasibility of AmBB fabrication at the laboratory scale, such as a COCA-like[5] or the UMACS[6] processes. The latter are based on powder metallurgy processes with ball-milling steps which generate large amounts of fine (sub-micronic) and highly contaminant radioactive particles.[5–8] Dustless processes are thus mandatory before planning a large-scale deployment.[9] Aiming the construction of dedicated facilities enabling to supply reactor needs, such as ASTRID, the development of an innovative route using micronic spherical precursors is studied. Through an adaptation of the weak acid resin (WAR) process,[10–13] the general approach consists in elaborating micronic and brittle spherical mixed-oxide precursors from ion exchange resin microspheres. These nanostructured soft agglomerates were developed to have the advantages of nano-powders, i.e. high reactivity during sintering step, without the major drawback of nanometric pulverulent compounds i.e. high dissemination capability during handling.[14] In complement, the spherical precursor geometry was chosen to facilitate the filling of the compaction chamber and subsequent pelletizing, leading to the final ceramic pellets. The final process is so called Calcined Resin Microsphere Pelletizing (CRMP) process and was already tested at the lab-scale as a feasible AmBB fabrication route.[15–17]

In the current CRMP process, the oxide microsphere synthesis is based on the fixation of americium (Am) and uranium (U) ions into ion exchange resin microspheres (~600 µm diameter). As-loaded microspheres are then converted to oxide during dedicated mineralization thermal treatments leading to the formation of porous oxide microspheres which are employed as pelletizing precursors. For this fabrication step, the resulting open microstructure of the oxide microspheres and thus the conversion step are the key elements. In the case of $U_{1-x}Am_xO_{2\pm\delta}$ synthesis from WAR process, two thermal treatments are required. The first one is performed under air until 973 K, for 1h, in order to evacuate the organic skeleton and to form an intermediary oxide mainly composed of $U_3O_8$. The second one, at 973 K during 4 h under reductive atmosphere (Ar-$H_2$ (4%)) aims to synthesize the final solid solution.[17] At the end, $U_{1-x}Am_xO_{2\pm\delta}$ microspheres presenting homogeneous and expanded microstructure are obtained as evidenced by SEM observations in Error! Reference source not found..

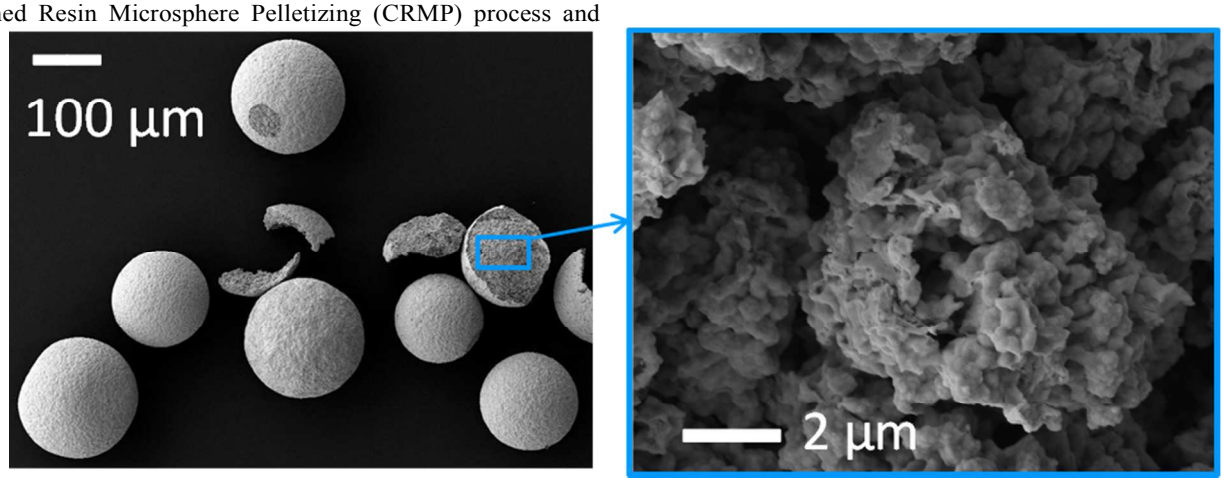


**Figure 1**. Secondary-electron SEM micrographs showing the oxide microsphere morphology and microstructure obtained after the reductive thermal treatment.

The objective is to control oxide microstructure and mechanical properties to allow microspheric precursor pelletizing and sintering into dense pellets (theoretical density (TD) > 95%).[2] Understanding $U_{1-x}Am_xO_{2\pm\delta}$ microsphere synthesis and particularly mechanisms implied during calcination leading to polymer skeleton combustion and the formation of the mixed oxide solid solution hence appears fundamental. This is the purpose of this article combining in-situ results obtained through XRD (X-Ray Diffraction) and, for the first time on Am-based samples, XAS (X-Ray Absorption Spectroscopy).

## Experimental

### Materials and methods

The employed poly-acrylic resin comes from the Dow Chemicals Company (Rohm and Haas, Chauny, France) and consists of an IMAC HP333 gel type acrylic exchanger in the form of porous resin microspheres. Concentrated ammonia solution (25%, Merck, Pro Analysis) and concentrated nitric acid solution (64%, Fisher Chemical, certified ACS Plus) were used in their diluted form (1 M) as washing solutions for resin pre-treatment before ion loading. Americium nitrate stock solution was prepared from the dissolution of $AmO_2$ in a 1M nitric acid solution. Uranium trioxide, obtained from the thermal conversion of ammonium diuranate was then dissolved progressively in the Am stock solution to neutralize excess of acidity, to raise pH with the formation of hydrolyzed uranyl species and to obtain the required stoichiometric proportions. The prepared loading solution corresponds to an ADUN (Acid Deficient Uranyl Nitrate) solution of pH 3.8, necessary to carry out exchange with a protonated acrylic exchanger.[18]

### Resin metal loading

A batch of resin microspheres presenting a preselected 630-800 µm diameter distribution was washed in a column by successive circulation of 1 M aqueous nitric acid solution, deionized water, 1 M aqueous ammonia solution, and finally deionized water, then only repeating the acid cycle a second time. This protocol was employed to remove cationic and chemical impurities potentially present in the microspheres after their industrial synthesis, as well as to convert the resin to its protonated form. As actinide ions can be fixed thanks to their substitution of $H^+$ species, pre-loading the acrylic resin with protons is a necessary step before cationic loading. The resin was then poured into a column with deionized water. The ADUN solution containing actinides in the U/Am ratio equal to 90/10 was recirculated through the column filled for approximately 4 h in order to reach equilibrium.[17] After achievment of equilibrium, the resin was washed with deionized water to remove ADUN solution from the resin pores, drained under vacuum and finally dried in a furnace at 373 K for 4 h. The initial stock and eluate solutions were analyzed by Thermal Ionization Mass Spectroscopy (TIMS) in order to determine the concentration of each cation, leading to the experimental stoichiometric ratio. After this last step for loaded resin fabrication, a first batch of microspheres was isolated for further characterizations, such as in-situ XAS. A second batch was calcined for 1 h at 973 K under air, following a heating rate of 5 $K.min^{-1}$. This calcination was performed in a tubular furnace (Lenton LTF), in which microspheres were disposed as a single layer in a quartz crucible. This second batch was especially dedicated to HT-XRD measurements under reductive atmosphere.

**X-Ray diffraction**

RT XRD diagrams were recorded at ATALANTE facility (CEA Marcoule) on powdered microspheres using a Bruker D8 Advance apparatus equipped with a Cu $K\alpha_{1,2}$ radiation and a linear Lynx-Eye detector, in a θ-θ Bragg–Brentano configuration. The step was of 0.02° with a time per step of 0.3 s, for an angular domain of 25 to 120° 2θ. The lattice parameter of the synthesized compound was determined using the Fullprof Suite software,[19,20] with a Le Bail method for refinements.[21]

**In-situ X-Ray diffraction**

HT-XRD diagrams were recorded on powdered microspheres using a Bruker D8 Advance apparatus equipped with a Cu $K\alpha_{1,2}$ radiation and a linear Lynx-Eye detector, in a θ-θ Bragg–Brentano configuration. The whole device is integrated in its own custom-built nitrogen-filled glove box dedicated to handling of nuclear materials at the LEFCA facility (CEA Cadarache).

The diffractometer is equipped with a heating stage from MRI Physikalische Gerate GmbH TC-Radiation of volume 0.5 L, allowing heating of the sample up to 2273 K. Under a reductive atmosphere, both a molybdenum strip as a direct heater and a tantalum radiant heater are used for temperature control.

The temperature was calibrated in steps of 100 K from RT to 1973 K, using a tungsten powder (Aldrich, 99.999%). The lattice parameters of tungsten determined as a function of the temperature were compared to those reported in the literature.[22,23] This temperature calibration was repeated several times, giving a constant temperature uncertainty of ± 15 K across the temperature range used.

Microspheres pre-calcined under air were used for this experiment. They were first ground with ethanol in an agate mortar. The grinding step was necessary before spreading on the Mo sample holder in order to obtain the homogeneous layer required for powder diffraction measurements.

Prior to the experiment, the Mo strip angular position and displacement were corrected. Before each experimental run, the specimen cell was purged with high-purity helium followed by a vacuum step of $10^{-5}$ mbar.

Powder diffraction diagrams were acquired by scanning from 18° to 142° 2θ. A counting time of 0.2 s per step and step intervals of 0.02° were used. Each XRD diagram was acquired in isothermal conditions from RT to 2023 K. The temperature step between each measurement was about 50 K. Heating rate between two temperatures was about 5 $K.s^{-1}$. During all measurements, the sample chamber atmosphere was maintained under flowing $He/H_2$ (5%) at a flow rate of 10 $L.h^{-1}$. The lattice parameter of the synthesized phase was determined using the Fullprof Suite software,[19,20] with a Le Bail method for refinements. [21]

**In-situ X-Ray Absorption Spectroscopy**

In-situ XAS measurements were performed at the INE (Institute for Nuclear Waste Disposal) beamline[24,25] of the ANKA synchrotron facility (Kalrsuhe Institute of Technology, Germany) under dedicated operating conditions (2.5 GeV, 120–150 mA). The incident ($I_0$) intensity was measured with an ionization chamber. The fluorescence photons were measured using a Ge solid-state detector. A Si(111) double-crystal monochromator coupled with collimating and focusing Rh-coated mirrors were used for energy selection. During measurements, the temperature of the sample was controlled using a dedicated micro furnace. Its sample holder, which is also the heating element, consists of a 1-mm-diameter Pt/Ir (90/10) wire with a 0.5-mm hole at its midpoint.[26,27] The whole configuration is inserted in a hermetic plastic box, preventing from contamination risk. In-situ XAS measurements were performed on a single (U,Am)-loaded-resin microsphere (before any thermal treatment) inserted in the hole. Spectra were recorded at the U $L_{III}$ and Am $L_{III}$ edges (17166 eV and 18510 eV respectively), focused on the XANES (X-ray absorption near edge structure) only. Energy calibration was performed with respect to the first inflection point of Y, Zr and Cr metal foils XANES spectrum collected before and after the in-situ experiment. Reference spectra for U and Am were collected at RT on $UO_2$, $U_4O_9$, $U_3O_8$, $AmO_2$ and on (U, Am) oxalate samples (15 at% of Am), using transmission pellets.

After a first RT measurement, a temperature cycle was performed, composed of successive isothermal plateaus at 600, 650, 750, 850 and 1000 K under air, conditions required to remove the organic matrix and obtain a highly reactive mixture.

Then the sample atmosphere was shifted to Ar and finally to Ar-$H_2$(4%) at 1000 K, with records at each transition. The last part of the cycle was composed of new isothermal plateaus at 1000, 1200 and 1400 K under the reductive atmosphere, to synthetize the solid solution, concluded by a last spectrum recorded after cooling down to RT. During each of these plateaus, at least two spectra were recorded for each edge. No significant deviations were observed between spectra at a given temperature. The furnace measurement chamber was under a static air atmosphere during the first part of the experiment, and under dynamic atmosphere when moving to Ar and Ar-$H_2$ (10 NL.$h^{-1}$), for a total volume of 0.4 L. XANES spectra were normalized using linear functions for pre- and post- edge modeling. White-line maximum were taken as the first zero-crossing of the first derivative. Pre-edge removal and normalization were performed using the ATHENA software.[28,29]

## Results and discussion

### Characterization of the loaded resin

The stock solution presented the desired target (90/10) ratio, before and after resin loading, indicating that the fixation was congruent: no selectivity from the poly-acrylic compound was observed between the U and Am cation loading. This result was confirmed by TIMS measurements of the dissolved oxide microspheres which allow us to evaluate the Am percentage versus heavy metals at 10.62±0.16 at%.

### In-situ XRD results

The in-situ XRD measurements were performed during the second step of the calcination of the (U,Am)-loaded resin. Indeed, the first calcination under air, already performed in the tubular furnace at 973 K, was necessary to remove carbon species and convert loaded resin microspheres into a first oxide mixture. The X-ray diagrams reporting crystallization under Ar-$H_2$(4%) atmosphere are presented in **Figure 2** and **Figure 3**. The first one is an isointensity map giving XRD diagram evolution as a function of the temperature. The second one, showing the main peaks of the two phases involved, focuses on the phase evolution.

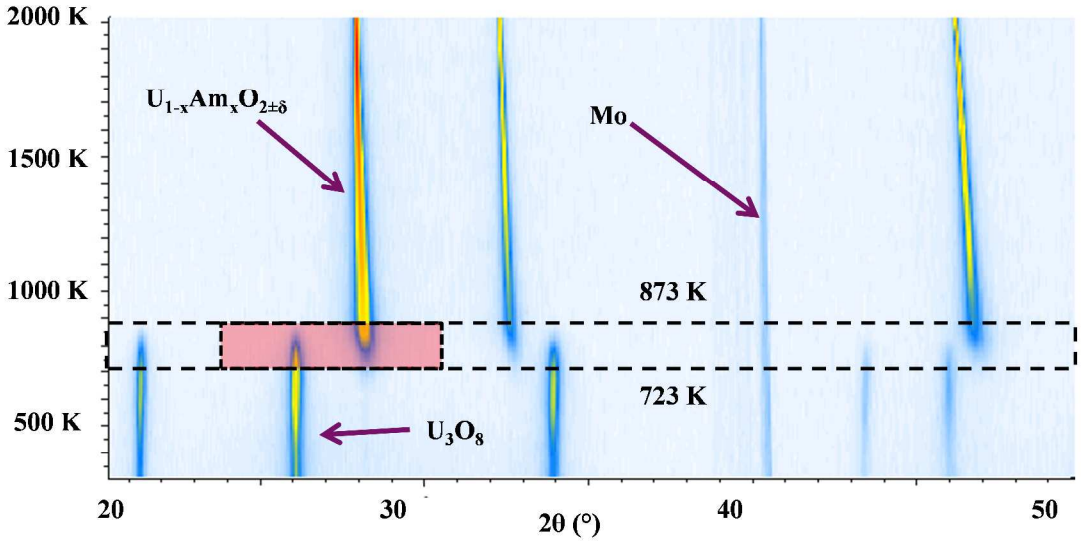


**Figure 2**. Isointensity map of the XRD diagrams as a function of temperature, recorded during the He-$H_2$ (5%) thermal treatment, illustrating the solid solution formation from (U,Am)$O_2$ microspheres coming from WAR process.

Dalton Transaction

RSCPublishing

ARTICLE

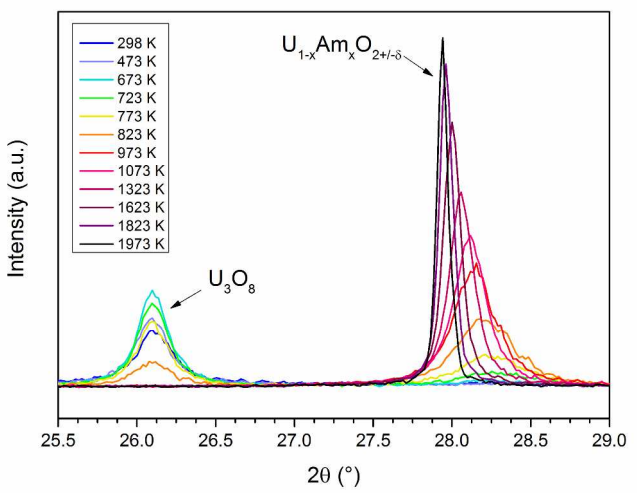


**Figure 3**. XRD diagrams, at different temperatures, showing the evolution of the $U_3O_8$ and $U_{1-x}Am_xO_{2\pm\delta}$ in a selected angle range (25.5-29°) - Background and $K\alpha_2$ contributions are removed with the EVA Diffrac$^{plus}$ software.

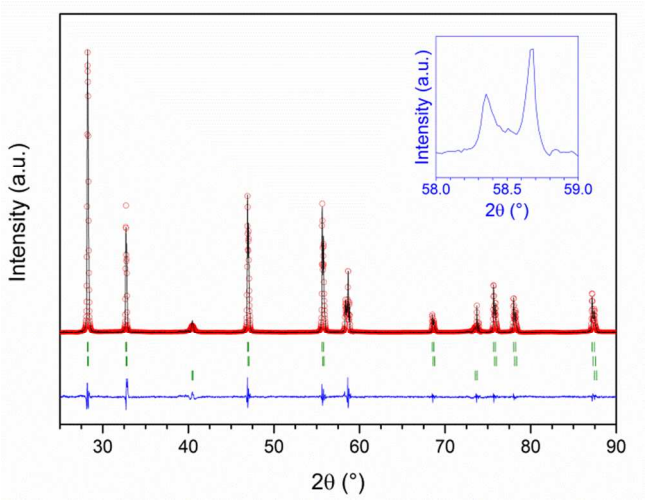


**Figure 4**. XRD diagram obtained after cooling down the sample used for HT-XRD from 2023 K to RT (50K.min$^{-1}$), under a reductive atmosphere (Ar-$H_2$ 4%) – Background and $K\alpha_2$ contributions are removed with the EVA Diffrac$^{plus}$ software – Experimental data are in black; calculated diagram is in red; difference between both is in blue; Bragg positions are presented in green – The blue insert shows the fluorite-phase peaks splitting into two.

**Figure 2** attests the sole presence of $U_3O_8$ in the intermediary oxide microspheres at RT, after oxidizing conversion and before reduction in temperature. In particular, no americium-based phases are detected on the first diagram recorded at RT. This fact is singular considering the Am/(U+Am) ratio of 10 at% in the starting microspheres, which is well enough to be detected by XRD (limit detection: beyond 2 at%).

The diagram recording during the heating step attest the formation of the solid solution from 723 K, temperature corresponding to the appearance of the first broad peaks characteristic of a fluorite-type structure. This can be precisely distinguished in **Figure 3**. From this temperature, the disappearance of the $U_3O_8$ main phase takes place in a 100 K-range, as the last main peak attesting its presence is recorded up to 873 K. At higher temperatures diagrams indicate the fluorite-type structure is the only phase characterizing the sample, as no additional crystallized phases are detected. The presence of the $U_{1-x}Am_xO_{2\pm\delta}$ solid solution is attested by the refinement of the lattice parameter. The direct formation of a monophasic compound differs from other synthesis processes implying solid state reaction between single oxides (e.g. UMACS), for which Am reduction was observed with the formation of $Am_2O_3$, before inter-diffusion with $UO_2$ and the synthesis of a solid solution.[30,31]

The lattice parameter determined at 2023 K was about 5.5767 ± 0.0004 Å. After cooling down to RT (cooling rate: 50 K.min$^{-1}$), the diagram obtained, reported in **Figure 4**, presents wide peaks in accordance with the presence of two phases.

The lattice parameter associated with the main phase is 5.4734 ± 0.0005 Å and that of the second one, 5.4660 ± 0.0005 Å. The appearance of a second phase during the cooling is most probably the consequence of an oxidation of the sample caused by the variations of oxygen partial pressure as a function of the temperature. The coexistence of these two phases can be explained by a low oxidation kinetic at RT, as it was previously reported.[32] Oxidation process starts from the surface of the particles to the bulk, as illustrated by the minor contribution of the smaller-lattice-parameter phase corresponding to the oxidized phase. A new diagram was recorded after 3 days of reoxidation, on another pellet fabricated with the same process. It is presented in **Figure 5**, and gives a lattice parameter of 5.4645 ± 0.0005 Å, in which a contribution of alpha-irradiation damages can be neglected.[33] This last value is lower than that of the oxidized phase of the in-situ XRD (5.4660 ± 0.0005 Å), indicating a higher oxidation degree of the sample three days after synthesis, meaning that the oxidation process continues for a few days. The sample finally obtained remains composed of a single fluorite-type phase.

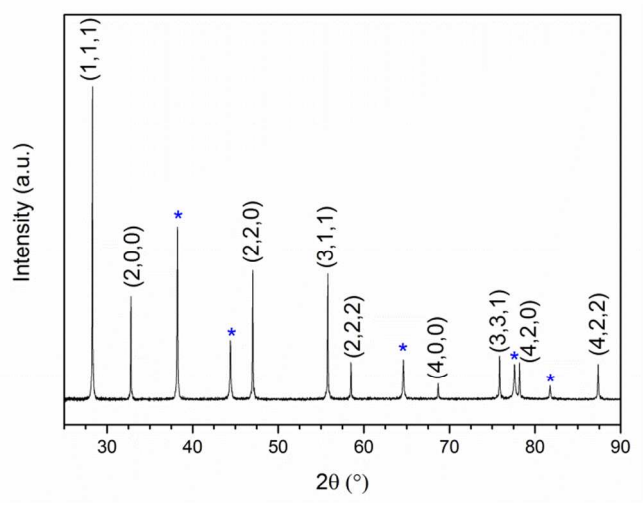


**Figure 5**. XRD diagram obtained from a CRMP pellet calcined until 2023 K under reductive atmosphere (Ar-$H_2$ 4%) and reoxidized 3 days before XRD measurements – the peaks matched with * correspond to Au phase mixed with the sample for 2θ position calibration - Background and $K\alpha_2$ contributions are removed with the EVA Diffrac$^{plus}$ software.

**In-situ XAS results**

The experiments performed on the (U,Am) loaded resin microspheres are divided in three main parts, so that the entire calcination cycle can be reproduced from the resin/polymeric state to the solid solution synthesis and existence. The presented spectra are compared, for $UL_{III}$ edge, with $U_3O_8$ ($U^{+V/+VI}$), $U_4O_9$ ($U^{+IV/+V}$) and $UO_2$ ($U^{+IV}$) references. The aspect of $U_3O_8$ spectrum is characterized by a WL like an important sinusoidal oscillation around 17181 eV. The reduction of U into $U^{+V}$ and $U^{+IV}$ can be detected by the progressive sharpening of the WL with a slight shift to lower energies, associated to the apparition of a second oscillation around 17220 eV. At $AmL_{III}$ edge, spectra are compared to $AmO_2$ for $Am^{+IV}$ and to $(U,Am)O_2$ solid solution obtained from oxalate co-conversion for $Am^{+III}$ reference. For comparison, the easiest way lies in the energy shift between the two WL bands.

All the white lines (WL) values are summarized in Table 1 and Table 2, for $UL_{III}$ and $AmL_{III}$ edges respectively. In this case, activation energies ($E_0$) will not be presented because of the presence of multiple valences for each sample oxidation state, inducing an important uncertainty on the $E_0$ determination, especially for U. This prevents from extracting relevant tendencies of $E_0$ values.

Table 1. Experimental values of WL extracted from XANES sample and reference spectra at $UL_{III}$ edge.

| Atmosphere | T (K) | WL (eV) |
|---|---|---|
| Air | RT | 17181.0(5) |
| | 600 | 17180.9(5) |
| | 650 | 17180.4(5) |
| | 850 | 17178.6(5) |
| | 1000 | 17179.0(5) |
| Argon | 1000 | 17178.8(5) |
| Ar-$H_2$ (4%) | 1000 | 17178.2(5) |
| | 1200 | 17178.5(5) |
| | 1400 | 17178.7(5) |
| | RT | 17179.0(5) |
| - | Ref $UO_2$ | 17177.6(5) |
| | Ref $U_4O_9$ | 17179.2(5) |
| | Ref $U_3O_8$ | 17181.2(5) |

Table 2. Experimental values of WL extracted from XANES sample and reference spectra at $AmL_{III}$ edge.

| Atmosphere | T (K) | WL (eV) |
|---|---|---|
| Air | RT | 18523.8(5) |
| | 600 | 18523.5(5) |
| | 650 | 18523.7(5) |
| | 750 | 18523.2(5) |
| | 850 | 18523.0(5) |
| | 1000 | 18523.1(5) |
| Argon | 1000 | 18522.5(5) |
| Ar-$H_2$ (4%) | 1000 | 18522.6(5) |
| | 1200 | 18523.5(5) |
| | 1400 | 18523.6(5) |
| | RT | 18523.2(5) |
| - | Ref $Am^{+IV}$ | 18525.2(5) |
| | Ref $Am^{+III}$ | 18523.0(5) |

The first XANES results that can be presented concern the thermal treatment performed under air, corresponding to the elimination of the organic skeleton until 1000 K. **Figure 6** and **Figure 7** show the XANES spectra recorded at different temperatures during the thermal cycle, at $UL_{III}$ and $AmL_{III}$ respectively.

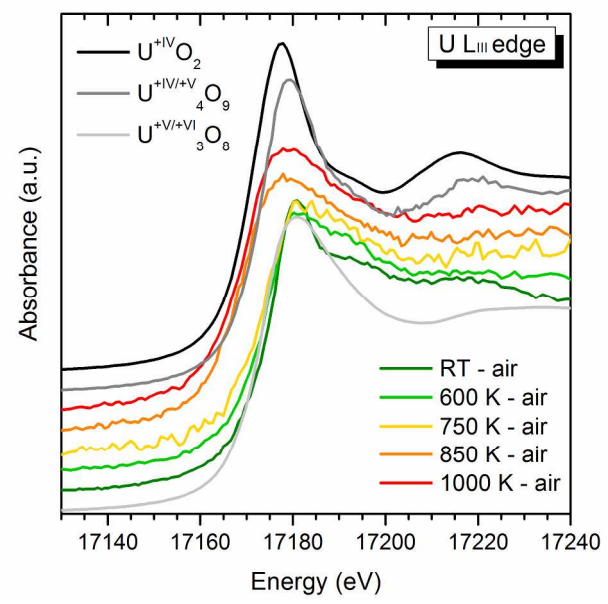


**Figure 6**. Normalized XANES spectra of the U-Am loaded resin microspheres from RT to 1000 K, under air, at $UL_{III}$ edge.

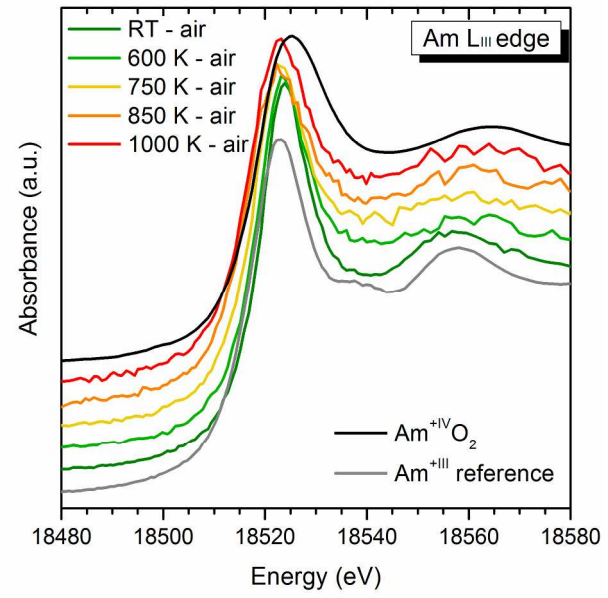


**Figure 7**. Normalized XANES spectra of the U-Am loaded resin microspheres from RT to 1000 K, under air, at $AmL_{III}$ edge.

Concerning U behavior, different steps can be noticed during the mineralization. From a WL point of view, spectra have similarities with $U_3O_8$ reference between RT and 750 K. This means that U is mostly present under the form $U^{(+V/+VI)}$ inside the sample. The rise of a second shoulder at higher energy (17220 eV), slightly appearing with temperature increase, attests the improvement of crystallinity with the formation of $U_3O_8$ instead of the original amorphous structure mostly composed of $U^{+VI}$ ions. From 850 K, a shift of the corresponding spectrum to smaller energies can be observed, also noticed with WL reading. It can be interpreted by an apparent reduction of the U species with the formation of $U^{+IV}$, added to $U^{+V}$ and $U^{+VI)}$, suggesting the formation of uranium oxide mixed with americium. $U^{+V/+VI}$ is still mainly present, with the preservation of the second first-mentioned shoulder at higher energy. Concerning Am behavior, first spectra until 600 K reveal the presence of mainly $Am^{+III}$, with a small proportion of $Am^{+IV}$, evidenced by a slight shift to higher energies. This corresponds to the domain in which the organic skeleton is oxidized and no crystalline structure can be identified through XRD measurements. Nevertheless, from 750 K, spectrum observation and WL comparison with $Am^{+III}$ reference reveal close results, attesting the presence of Am with a single +III oxidation state.

The second part of the experiment consisted in changing the atmosphere from a static oxidizing atmosphere to a dynamic reductive one. This modification was performed progressively in order to ensure that the microsphere was not submitted to important constraints or gas flow. Firstly, pure Ar was sent inside the chamber, at 5 then 10 $NL.h^{-1}$. XANES spectra (at $UL_{III}$ and $AmL_{III}$ edges each) were recorded at this intermediary state, and then Ar-$H_2$ (4%) was flowed inside the furnace at 10 $NL.h^{-1}$. All this protocol was performed at 1000 K. **Figure 8** and **Figure 9** present the XANES spectra recorded at 1000 K under the different atmospheres, for $UL_{III}$ and $AmL_{III}$ respectively.

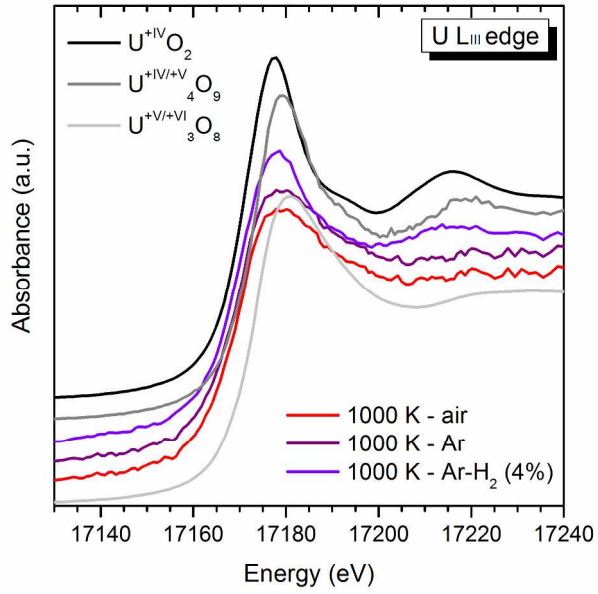


**Figure 8**. Normalized XANES spectra of the U-Am loaded resin microspheres at 1000 K under three different and consecutive atmospheres – air, argon, Ar-$H_2$ (4%) – at $UL_{III}$ edge.

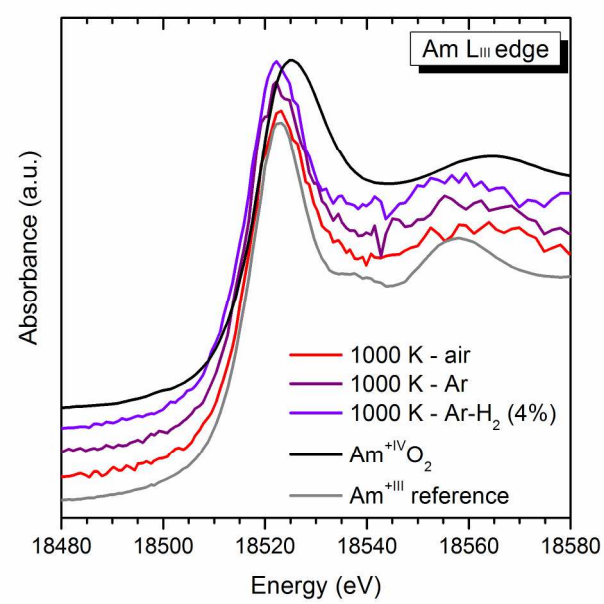


**Figure 9**. Normalized XANES spectra of the U-Am loaded resin microspheres at 1000 K under three different and consecutive atmospheres – 1/ air; 2/ Argon; 3/ Ar-$H_2$ (4%) – at $AmL_{III}$ edge.

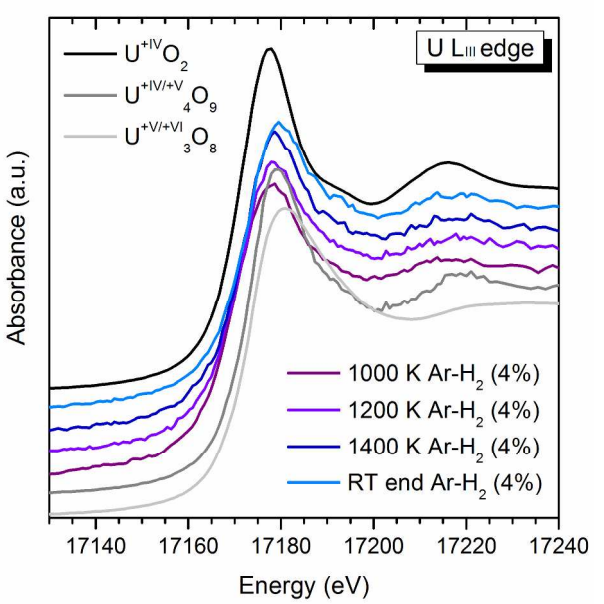


**Figure 10**. Normalized XANES spectra of the U-Am loaded resin microspheres from 1000 K to 1400 K, under Ar-H2 (4%), at ULIII edge

Concerning $UL_{III}$ edge, progressive sharpening of the U WL can be noticed with the introduction of a neutral (Ar) then reductive atmosphere (Ar-$H_2$). This can be interpreted as a reduction of uranium cations, with removal of oxidative atmosphere, which could enable the formation of a local structure close to that of a fluorine-type one. Concerning Am oxidation state, no change occurs during the gas shift, and it remains only present as $Am^{+III}$.

The third and last part of the XAS experiments was to collect data during the temperature increase under a reductive atmosphere. Spectra were recorded until 1400 K and after cooling down to RT. **Figure 10** and **Figure 11** show the evolution of the normalized spectra with the temperature.

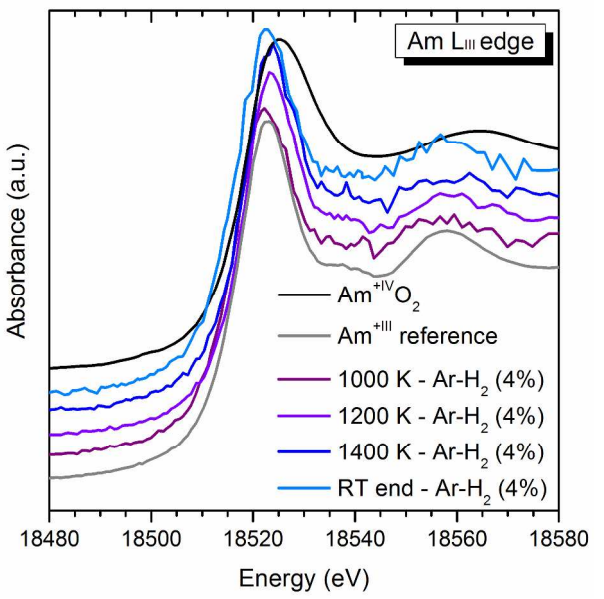


**Figure 11**. Normalized XANES spectra of the U-Am loaded resin microspheres from 1000 K to 1400 K, under Ar-$H_2$ (4%), at $AmL_{III}$ edge.

By related them with the WL values on Table 1 and Table 2, it can be concluded that U and Am species are present at a reduced state under high temperature, as well as at RT. U is present as $U^{(+IV/+V)}$ while Am remains only present as $Am^{+III}$. This cationic charge distribution is similar to the one already observed for other studied $U_{1-x}Am_xO_{2\pm\delta}$ solid solution, obtained from different synthesis processes.[5,34] Results were determined during previous experiments at 20 K during ex-situ XAS experiments (ESRF, Rossendorf Beam Line). It can be

concluded, that in this new range of high temperatures (1400 K), considering these thermodynamic conditions, U is still present under a mixed oxidation state, allowing electroneutrality conservation inside the crystalline structure with a trivalent Am and a mixed valence for U (+IV/V), in the same way as that observed at 20 K. The experimental observation of the reductive state at HT is for the first-time mentioned, thanks to the new in-situ XAS measurements on MA.

**Comparison and correlation between in-situ XAS and XRD results**

Combination between HT-XRD and in-situ XAS results is helpful for a better understanding of the oxides present under the two different atmospheres. Indeed, no Am-bearing crystalline phases are detected by XRD during the first oxidation stage, whereas its presence, mostly as $Am^{+III}$, is noticed through XANES analysis. The reduction observed from 850 K under air of a significant part of uranium $U^{+IV}$ could help to explain the Am absence on the intermediary oxide XRD diagram with the potential formation of nano-domains of an intermediate $U_{1-x}Am_xO_{2\pm\delta}$ phase (presenting a higher Am content than the selected cationic stoichiometry) from 850 K under air. Such domains would not be detected by XRD due to too short coherent length, but would be assessed by XAS analysis, which is able to probe all the target elements (U or Am in the present case) in the sample, independently of their presence in a crystalline or amorphous phase. This hypothesis would also justify the presence of $Am^{+III}$ despite the oxidizing atmosphere used, under which americium is expected to be present as $Am^{+IV}$.[35,36] As it was previously reported, notably by XAS, Am remains present at a reduced state in $U_{1-x}Am_xO_{2\pm\delta}$ compounds (for Am/(U+Am) ratios comprised between 5 and 20 at%). A similar charge repartition could be thus expected in these nano-domains.

## Conclusions

This study has been well participating in the progress of AmBB fabrication mastery and is included in the transmutation program as an important new key work. The $U_{1-x}Am_xO_{2\pm\delta}$ solid solution formation via ion exchange resin microsphere calcination (WAR process) was investigated by in-situ XRD and XAS, in order to better understand the mineralization step and the mechanisms implied during the oxide crystallization. XRD gave information on the key temperatures of the solid solution synthesis during the reductive thermal treatment. 723 K can be remembered as the temperature at which the first wide peaks corresponding to a fluorite-type structure are identified, meaning $U_{1-x}Am_xO_{2\pm\delta}$ solid solution appearance. On contrary, 873 K is the temperature at which the last peak of the intermediate $U_3O_8$ phase is observed without Am presence, corresponding to the synthesis of the final synthesis of the $U_{0.8}Am_{0.2}O_{2\pm\delta}$ compound. In-situ XAS allowed the determination of the oxidation states of U and Am during the whole mineralization from the amorphous resin state to the obtaining of the selected mixed-oxide. To summarize, during oxidative thermal treatment, $U^{+V/VI}$ and mainly $Am^{+III}$ are observed, with a small presence of $Am^{+IV}$ until 850 K. From this temperature, a slight reduction of a part of U can be pointed out with the apparition of $U^{+IV}$, while Am becomes only trivalent. Then, results concern the transition to a reductive atmosphere required for the solid solution formation from 1000 K to 1400 K. The reduction of U into $U^{+IV/V}$ and the upholding of Am into $Am^{+III}$ are assessed, as well as for the cooling down to RT.

The correlation between in-situ XAS and XRD allows raising a hypothesis concerning the missing Am after the oxidative treatment, from an XRD point of view, while it is detected as mainly trivalent through XAS measurements. The oxidation state taken by U from 850 K would help to explain it through the reduction of a part of it into $U^{+IV/V}$. Indeed it could correspond to the formation of nano-domains of $U_{1-x}Am_xO_{2\pm\delta}$ from 850 K under air, first beginning of the solid solution formation.

The first in-situ XAS measurements performed on U and Am gave novel results concerning the behavior of $U_{1-x}Am_xO_{2\pm\delta}$ solid solution and its formation through the WAR process. Besides, these results, associated to the solid solution cationic charge repartition at HT, are new data of importance for such radioactive materials, as it is the first XAS experiment involving U and Am heated up to 1400 K, previous data being only collected at 20 K in cryostat. They will be implemented in the thermodynamic data base called "fuel base"[37] in order to develop the still unknown U-Am-O ternary phase diagram, required for AmBB fabrication, $(U,Am)O_2$ storage in various conditions, and more generally for better knowledge of irradiation and safety studies on $(U,Am)O_2$ compounds.

## Acknowledgements

The authors thank M. Bataille , L. Ramond and P. Coste for in-situ XAS measurements; J.-C. Richaud from the LEFCA for in-situ XRD recordings; A. Gauthé, I. Jobelin, P. Grangaud and J.-M. Pomarede for sample synthesis; S. Caron for SEM analysis; CEA/MAR/DRCP/SE2A/LAMM for TIMS measurements. We acknowledge the ANKA Synchrotron Light Source and the FP7 Talisman program for provision of beamtime at the INE beamline and for assistance in setting up the in-situ XAS measurement system. M. Caisso and F. Lebreton are grateful for Ph.D. fellow-ship funding by the CEA PACFA program. XAS in situ experi-ment developments were funded by the NEEDS program.

## Notes and references

[1]*CEA, DEN, DTEC/SDTC/LEMA, F-30207 Bagnols-sur-Cèze Cedex, France.*
[2]*CEA, DEN, DRCP/SERA/LCAR, F-30207 Bagnols-sur-Cèze Cedex, France*
[3]*CEA, DEN, DEC/SPUA/LMPC, F-13108 Saint-Paul-Lez-Durance Cedex, France*
[4]*CEA, DEN, DEC/SESC/LLCC, F-13108 Saint-Paul-Lez-Durance Cedex, France*

[5]*Karlsruhe Institute of Technology, Institute for Nuclear Waste Disposal (KIT-INE), Hermann-von-Helmholtz-Platz 1, D-76344 Eggenstein-Leopoldshafen, Germany*
[6]*Institut de Physique du Globe de Paris-CNRS, Géochimie & Cosmochimie, 1 rue Jussieu, 75005 Paris, France*
[7]*Institut Européen des Membranes, UMR 5635 CNRS-ENSCM-UM2, CC047, Université Montpellier 2, F-34095 Montpellier Cedex 5, France*

Corresponding author : * Dr. Thibaud Delahaye; thibaud.delahaye@cea.fr; 0033466796542.

1. F. Gauche and J. Rouault, *Energy Procedia*, 2011, **7**, 314–316.
2. D. Warin, *J. Nucl. Sci. Technol.*, 2007, **44**, 410–414.
3. S. Vaudez, R. C. Belin, L. Aufore, P. Sornay and S. Grandjean, *J. Nucl. Mater.*, 2013, **442**, 227–234.
4. J.-P. Grouiller, S. Pillon, C. de Saint Jean, F. Varaine, L. Leyval, G. Vambenepe and B. Carlier, *J. Nucl. Mater.*, 2003, **320**, 163–169.
5. D. Prieur, A. Jankowiah, T. Delahaye, N. Herlet, P. Dehaudt and P. Blanchart, *J. Nucl. Mater.*, 2011, **414**, 503–507.
6. T. Delahaye, F. Lebreton, D. Horlait, N. Herlet and P. Dehaudt, *J. Nucl. Mater.*, 2013, **432**, 305–312.
7. D. Prieur, F. Lebreton, P. M. Martin, A. Jankowiak, T. Delahaye, P. Dehaudt and P. Blanchart, *J. Eur. Ceram. Soc.*, 2012, **32**, 1585–1591.
8. F. Lebreton, D. Prieur, A. Jankowiak, M. Tribet, C. Leorier, T. Delahaye, L. Donnet and P. Dehaudt, *J. Nucl. Mater.*, 2012, **420**, 213–217.
9. D. Horlait, F. Lebreton, A. Gauthé, M. Caisso, B. Arab-Chapelet, S. Picart and T. Delahaye, *J. Nucl. Mater.*, 2014, **444**, 181–185.
10. 3.800.023, 1974.
11. G. W. Weber, R. L. Beatty, V. J. Tennery, 1977.
12. S. Picart, H. Mokhtari, I. Ramière and I. Jobelin, *IOP Conf. Ser. Mater. Sci. Eng.*, 2010, **9**, 012025.
13. M. S. Wilson, A. Delariva and F. H. Garzon, *J. Mater. Chem.*, 2011, **21**, 7418–7424.
14. M. Caisso, F. Lebreton, D. Horlait, S. Picart, P. M. Martin, R. Bès, C. Renard, P. Roussel, D. R. Neuville, K. Dardenne, J. Rothe, T. Delahaye and A. Ayral, *J. Solid State Chem.*, 2014, **218**, 155–163.
15. E. Remy, S. Picart, S. Grandjean, T. Delahaye, N. Herlet, P. Allegri, O. Dugne, R. Podor, N. Clavier, P. Blanchart and A. Ayral, *J. Eur. Ceram. Soc.*, 2012, **32**, 3199–3209.
16. E. Remy, S. Picart, T. Delahaye, I. Jobelin, O. Dugne, I. Bisel, P. Blanchart and A. Ayral, *J. Nucl. Mater.*, 2014, **448**, 80–86.
17. E. Remy, S. Picart, T. Delahaye, I. Jobelin, F. Lebreton, D. Horlait, I. Bisel, P. Blanchart and A. Ayral, *J. Nucl. Mater.*, 2014, **453**, 214–219.
18. K. J. NOTZ, P. A. HAAS and J. H. SHAFFER, *Radiochim. Acta*, 1978, **25**, 153–160.
19. J. R. Carjaval, *Satell. Meet. Powder Diffr. XV IUCr Congr.*, 1990.
20. J. Rodríguez-Carvajal, *Phys. B Condens. Matter*, 1993, **192**, 55–69.
21. A. Le Bail, *Powder Diffr.*, 2005, **20**, 316–326.
22. L. S. Dubrovinsky and S. K. Saxena, *Phys. Chem. Miner.*, 1997, **24**, 547–550.
23. K. Wang and R. R. Reeber, *Mater. Sci. Eng. R Rep.*, 1998, **23**, 101–137.
24. J. Rothe, M. A. Denecke, K. Dardenne and T. Fanghänel, *Radiochim. Acta*, 2006, **94**, 691–696.
25. K. Dardenne, B. Brendebach, M. A. Denecke, X. Liu, J. Rothe and T. Vitova, *J. Phys. Conf. Ser.*, 2009, **190**, 012037–012037/4.
26. V. Magnien, D. R. Neuville, L. Cormier, J. Roux, J.-L. Hazemann, D. de Ligny, S. Pascarelli, I. Vickridge, O. Pinet and P. Richet, *Geochim. Cosmochim. Acta*, 2008, **72**, 2157–2168.
27. D. R. Neuville, L. Cormier, V. Montouillout, P. Florian, F. Millot, J.-C. Rifflet and D. Massiot, *Am. Mineral.*, 2008, **93**, 1721–1731.
28. M. Newville, *J. Synchrotron Radiat.*, 2001, **8**, 322–324.
29. B. Ravel and M. Newville, *J. Synchrotron Radiat.*, 2005, **12**, 537–541.
30. F. Lebreton, R. C. Belin, D. Prieur, T. Delahaye and P. Blanchart, *Inorg. Chem.*, 2012, **51**, 9369–9375.
31. F. Lebreton, R. C. Belin, T. Delahaye and P. Blanchart, *J. Solid State Chem.*, 2012, **196**, 217–224.
32. D. Horlait, F. Lebreton, P. Roussel and T. Delahaye, *Inorg. Chem.*, 2013, **52**, 14196–14204.
33. F. Lebreton, P. Martin, D. Horlait and R. Bès, *Eur. J. Inorg. Chem.*, 2014.
34. D. Prieur, P. Martin, F. Lebreton, T. Delahaye, D. Banerjee, A. C. Scheinost and A. Jankowiak, *J. Nucl. Mater.*, 2013, **434**, 7–16.
35. S. Casalta, H. Matzke and C. Prunier, in *Proceedings Global 95*, Versailles, France, 1995.
36. S. Casalta, Université d'Aix-Marseille I, 1996.
37. C. Guéneau, A. Chartier and L. Van Brutzel, in *Comprehensive Nuclear Materials*, ed. R. J. M. Konings, Elsevier, Oxford, 2012, pp. 21–59.



 

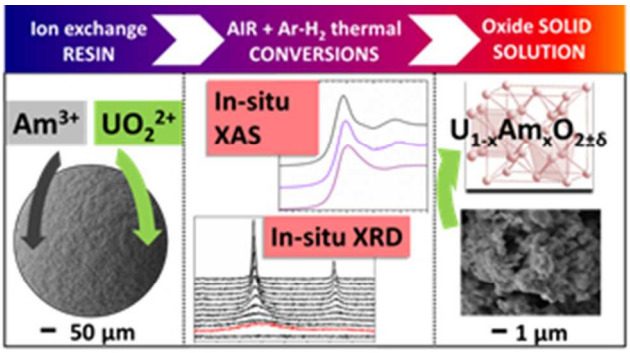


113x73mm (72 x 72 DPI)